

An Effective Model of the Retinoic Acid Induced HL-60 Differentiation Program

Ryan Tasseff, Holly A. Jensen, Wei Dai, Rodica P. Bunaciu[†], Johanna Congleton[†], Andrew Yen[†], and Jeffrey D. Varner*

Robert Frederick Smith School of Chemical and Biomolecular Engineering and [†]Department of Biomedical Sciences, Cornell University, Ithaca NY 14853

Running Title: Effective modeling of HL-60 differentiation

To be submitted: *Frontiers in Systems Biology*

*Corresponding author:

Jeffrey D. Varner,

Professor, Robert Frederick Smith School of Chemical and Biomolecular Engineering,
244 Olin Hall, Cornell University, Ithaca NY, 14853

Email: jdv27@cornell.edu

Phone: (607) 255 - 4258

Fax: (607) 255 - 9166

Abstract

In this study, we present an effective model All-Trans Retinoic Acid (ATRA)-induced differentiation of HL-60 cells. The model describes a key architectural feature of ATRA-induced differentiation, positive feedback between an ATRA-inducible signalsome complex involving many proteins including Vav1, a guanine nucleotide exchange factor, and the activation of the mitogen activated protein kinase (MAPK) cascade. The model, which was developed by integrating logical rules with kinetic modeling, was significantly smaller than previous models. However, despite its simplicity, it captured key features of ATRA induced differentiation of HL-60 cells. We identified an ensemble of effective model parameters using measurements taken from ATRA-induced HL-60 cells. Using these parameters, model analysis predicted that MAPK activation was bistable as a function of ATRA exposure. Conformational experiments supported ATRA-induced bistability. These findings, combined with other literature evidence, suggest that positive feedback is central to a diversity of cell fate programs.

1 Introduction

2 Understanding the architecture of differentiation programs is an important therapeutic
3 challenge. Differentiation induction chemotherapy (DIC), using agents such as the vita-
4 min A derivative all-trans retinoic acid (ATRA), is a promising approach for the treatment
5 of many cancers (1–3). For example, ATRA treatment induces remission in 80–90% of
6 promyelocytic leukemia (APL) PML-RAR α -positive patients (4), thereby transforming a
7 fatal diagnosis into a manageable disease. However, remission is sometimes not durable
8 and relapsed cases exhibit emergent ATRA resistance (5, 6). To understand the basis of
9 this resistance, we must first understand the ATRA-induced differentiation program. To-
10 ward this challenge, lessons learned in model systems, such as the lineage-uncommitted
11 human myeloblastic cell line HL-60, could inform our analysis of the more complex dif-
12 ferentiation programs occurring in patients. Patient derived HL-60 leukemia cells have
13 been a durable experimental model since the 1970's to study differentiation (7). HL-60
14 undergoes cell cycle arrest and either myeloid or monocytic differentiation following stim-
15 ulation; ATRA induces G1/G0-arrest and myeloid differentiation in HL-60 cells, while 1,25-
16 dihydroxy vitamin D3 (D3) induces arrest and monocytic differentiation. Commitment to
17 cell cycle arrest and differentiation requires approximately 48 hr of treatment, during which
18 HL-60 cells undergo two division cycles.

19 Sustained mitogen-activated protein kinase (MAPK) activation is a defining feature of
20 ATRA-induced HL-60 differentiation. ATRA drives sustained MEK-dependent activation
21 of the Raf/MEK/ERK pathway, leading to arrest and differentiation (8). MEK inhibition re-
22 sults in the loss of ERK and Raf phosphorylation, and the failure to arrest and differentiate
23 (9). ATRA (and its metabolites) are ligands for the hormone activated nuclear transcrip-
24 tion factors retinoic acid receptor (RAR) and retinoid X receptor (RXR) (10). RAR/RXR
25 activation is necessary for ATRA-induced Raf phosphorylation (9), and the formation of
26 an ATRA-inducible signalsome complex at the membrane which drives MAPK activation

27 through a yet to be identified kinase activity. While the makeup of the signalsome com-
28 plex is not yet known, we do know that it is composed of Src family kinases Fgr and Lyn,
29 PI3K, c-Cbl, Slp76, and KSR, as well as IRF-1 transcription factors (11–15). Signalsome
30 formation and activity is driven by ATRA-induced expression of CD38 and the putative
31 heterotrimeric Gq protein-coupled receptor BLR1 (16, 17). BLR1, identified as an early
32 ATRA (or D3)-inducible gene using differential display (18), is necessary for MAPK ac-
33 tivation and differentiation (17), and is also involved with signalsome activity. Studies
34 of the BLR1 promoter identified a 5' 17bp GT box approximately 1 kb upstream of the
35 transcriptional start that conferred ATRA responsiveness (17). Members of the BLR1
36 transcriptional activator complex, e.g. NFATc3 and CREB, are phosphorylated by ERK,
37 JNK or p38 MAPK family members suggesting positive feedback between the signal-
38 some and MAPK activation (19). BLR1 overexpression enhanced Raf phosphorylation
39 and accelerated terminal differentiation, while Raf inhibition reduced BLR1 expression
40 and differentiation (20). BLR1 knock-out cells failed to activate Raf or differentiate in
41 the presence of ATRA (20). Interestingly, both the knockdown or inhibition of Raf, also
42 reduced BLR1 expression and functional differentiation (20). Thus, the expression of
43 signalsome components e.g., BLR1 was Raf dependent, while Raf activation depended
44 upon the signalsome. A recent computational study of ATRA-induced differentiation in
45 HL-60 cells suggested that the BLR1-MAPK positive feedback circuit was sufficient to ex-
46 plain ATRA-induced sustained MAPK activation, and the expression of a limited number
47 of functional differentiation markers (21). Model analysis also suggested that Raf was the
48 most distinct of the MAPK proteins. However, this previous study developed and analyzed
49 a complex model, thus leaving open the critical question of what is the minimal positive
50 feedback circuit required to drive ATRA-induced differentiation.

51 In this study, we explored this question using a minimal mathematical model of the
52 key architectural feature of ATRA induced differentiation of HL-60 cells, namely positive

53 feedback between an ATRA-inducible signalsome complex and MAPK activation. The
54 ATRA responsive signalsome-MAPK circuit was then used to drive a downstream gene
55 expression program which encoded for the expression of functional differentiation mark-
56 ers. The effective model used a novel framework which integrated logical rules with ki-
57 netic modeling to describe gene expression and protein regulation, while largely relying
58 upon biophysical parameters from the literature. This formulation significantly reduced
59 the size and complexity of the model compared to the previous study of Tasseff et al.,
60 while increasing the breadth of the biology described (21). The effective model, despite
61 its simplicity, captured key features of ATRA induced differentiation of HL-60 cells. Model
62 analysis predicted the bistability of MAPK activation as a function of ATRA exposure; con-
63 formational experiments supported ATRA-induced bistability. Model simulations were also
64 consistent with measurements of the influence of MAPK inhibitors, and the failure of BLR1
65 knockout cells to differentiate when exposed to ATRA. Lastly, we showed by through im-
66 munoprecipitation studies, that the guanine nucleotide exchange factor Vav1 is potentially
67 a new ATRA-inducible member of the siganlsome complex. Taken together, these findings
68 when combined with other literature evidence, suggested that positive feedback architec-
69 tures are central to differentiation programs generally, and necessary for ATRA-induced
70 differentiation.

71 **Results**

72 We constructed an effective model of ATRA-induced HL-60 differentiation which described
73 signaling and gene expression events following the addition of ATRA (Fig. 1). The model
74 connectivity was developed from literature and the studies presented here (Table ZZ). We
75 decomposed the ATRA program into three modules; a signal initiation module that sensed
76 and transformed the ATRA signal into activated cRaf-pS621 and the ATRA-RXR/RAR
77 (Trigger) signals (Fig. 1A); a signal integration module that controlled the expression of
78 upstream transcription factors given cRaf-pS621 and activated Trigger signals (Fig. 1B);
79 and a phenotype module which encoded the expression of functional differentiation mark-
80 ers from the ATRA-inducible transcription factors (Fig. 1C). Each component of these
81 modules was described by a mRNA and protein balance equation. Additionally, the sig-
82 nal initiation module also described the abundance of activated species e.g., Trigger and
83 cRaf-pS621 whose values were derived from unactivated Trigger and cRaf protein levels.
84 Lastly, because the population of HL-60 cells was dividing (at least before ATRA-induced
85 cell cycle arrest), we also considered a dilution term in all balance equations. The sig-
86 nal initiation module contained nine differential equations, while the signal integration and
87 phenotype modules were collectively encoded by 54 differential equations. Model pa-
88 rameters were taken literature, or estimated from experimental data taken from literature
89 using heuristic optimization (see materials and methods).

90 The signal initiation module recapitulated sustained signalsome and MAPK activation
91 following exposure to $1\mu\text{M}$ ATRA (Fig. 2A-B). An ensemble of effective model param-
92 eters was estimated by minimizing the difference between simulations and time-series
93 measurements of BLR1 mRNA and cRaf-pS621 following the addition of $1\mu\text{M}$ ATRA. We
94 focused on the S621 phosphorylation site of cRaf since enhanced phosphorylation at
95 this site is a defining characteristic of sustained MAPK activation in HL-60. The effective
96 model captured both ATRA-induced BLR1 expression (Fig. 2A) and sustained phospho-

97 phosphorylation of cRaf-pS621 (Fig. 2B) in a growing population of HL-60 cells. Together, the
98 reinforcing positive feedback between the signalsome and MAPK led to sustained activation
99 over multiple cellular generations. However, the effective model failed to capture the
100 decline of BLR1 message after 48 hr of ATRA exposure. This suggested that we captured
101 the logic leading to the onset of differentiation, but failed to describe program shutdown.
102 Next, we tested the response of the signal initiation module to different ATRA dosages.

103 The signal initiation model was bistable with respect to ATRA induction (Fig. 2C-D).
104 Phaseplane analysis predicted two stable steady-states when ATRA was present below
105 a critical threshold (Fig. 2C). In the lower stable state, neither the signalsome nor cRaf-
106 pS621 were present (thus, the differentiation program was deactivated). However, at
107 the high stable state, both the signalsome and cRaf-pS621 were present, allowing for
108 sustained activation and differentiation. Interestingly, when ATRA was above a critical
109 threshold, only the activated state was accessible (Fig. 2D). To test these findings, we
110 first identified the ATRA threshold. We exposed HL-60 cells to different ATRA concen-
111 trations for 72 hr (Fig. 2E). Morphological changes associated with differentiation were
112 visible for ATRA $\geq 0.25 \mu\text{M}$, suggesting the critical ATRA threshold was near this concen-
113 tration. Next, we conducted ATRA washout experiments to determine if activated cells
114 remained activated in the absence of ATRA. HL-60 cells locked into an activated state
115 remained activated following ATRA withdraw (Fig. 3). This sustained activation resulted
116 from reinforcing feedback between the signalsome and the MAPK pathway. Thus, follow-
117 ing activation, if we inhibited or removed elements from the signal initiation module we
118 expected the siganlsome and MAPK signals to decay. We simulated ATRA induced acti-
119 vation in the presence of kinase inhibitors, and without key circuit elements. Consistent
120 with experimental results using multiple MAPK inhibitors, ATRA activation in the presence
121 of MAPK inhibitors lowered the steady-state value of signalsome (Fig. 3A). In the pres-
122 ence of BLR1, the signalsome and cRaf-pS621 signals were maintained following ATRA

123 withdraw (Fig. 3B, gray). On the other hand, BLR1 deletion removed the ability of the
124 circuit to maintain a sustained MAPK response following the withdraw of ATRA (Fig. 3B,
125 blue). Lastly, washout experiments in which cells were exposed to $1\mu\text{M}$ ATRA for 24 hr,
126 and then transferred to fresh media without ATRA, confirmed the persistence of the self
127 sustaining activated state for up to 144 hr (Fig. 3C). Thus, these experiments confirmed
128 that reinforcing positive feedback likely drives the ATRA-induced differentiation program.
129 Next, we analyzed the ATRA-induced downstream gene expression program following
130 signalsome and cRaf activation.

131 The signal integration and phenotype modules described ATRA-induced gene expres-
132 sion events in wild-type HL-60 cells (Fig. 4). The signal initiation module produced two
133 outputs, activated Trigger and cRaf-pS621 which drove the expression of ATRA-induced
134 transcription factors, which then in turn activated the phenotypic program. In particular,
135 Trigger, which is a surrogate for the RAR α /RXR transcriptional complex, regulated the ex-
136 pression of the transcription factors CCATT/enhancer binding protein α (C/EBP α), PU.1,
137 and EGR1. In turn, these transcription factors, in combination with cRaf-pS621, regulated
138 the expression of downstream phenotypic markers such as CD38, CD11b or P47Phox.
139 We assembled the connectivity of the signal integration and phenotypic programs driven
140 by Trigger and cRaf-pS621 from literature (Table ZZ). We estimated the parameters which
141 appeared in the control laws regulating these programs from steady-state and dynamic
142 measurements of transcription factor and phenotypic marker expression following the ad-
143 dition of ATRA [REFHERE]. However, the bulk of the remaining model parameters were
144 taken from directly from literature [REFHERE] and were not estimated in this study (see
145 materials and methods). The model simulations captured the time dependent expression
146 of CD38 and CD11b following the addition ATRA (Fig. 4A), and the steady-state for sig-
147 nal integration and phenotypic markers (Fig. 4B). Taken together, the signal integration
148 and phenotypic simulations were consistent with measurements, thereby validating the

149 assumed molecular connectivity.

150 The composition of the siganlsome, and the kinase ultimately responsible for medi-
151 ating ATRA-induced Raf activation is currently unknown. To explore this question, we
152 conducted immunoprecipitation and subsequent Western blotting to identify physical in-
153 teractions between Raf and 19 putative interaction partners. A panel of 19 possible Raf
154 interaction partners (kinases, GTPases, scaffolding proteins etc) was constructed based
155 upon known signaling pathways. We did not consider the most likely binding partner, the
156 small GTPase RAS, as previous studies have ruled it out in MAPK activation in HL-60 cells
157 (20, 22). Total Raf was used as a bait protein for the immunoprecipitation studies. Interro-
158 gation of the Raf interactome suggested Vav1 was involved with ATRA-induced initiation
159 of MAPK activity (Fig. 5). Western blot analysis using total Raf and pS621 Raf specific
160 antibodies confirmed the presence of the bait protein, total and phosphorylated forms, in
161 the immunoprecipitate (Fig. 5A). Of the 19 proteins sampled, Vav1, Src, CK2, Akt, and
162 14-3-3 precipitated with Raf, suggesting a direct physical interaction was possible. How-
163 ever, only the associations between Raf and Vav1 and Raf and Src were ATRA-inducible
164 (Fig. 5). Furthermore, the Vav1 and Src associations were correlated with pS621 Raf
165 abundance in the precipitate. Others proteins e.g., CK2, Akt and 14-3-3, generally bound
166 Raf regardless of phosphorylation status or ATRA treatment. The remaining 14 proteins
167 were expressed in whole cell lysate (Fig. 5B), but were not detectable in the precipitate
168 of Raf IP. Treatment with the Raf kinase inhibitor GW5074 following ATRA exposure re-
169 duced the association of both Vav1 with Raf and Src with Raf (Fig. 5), although the signal
170 intensity for Src was notably weak. However, GW5074 did not influence the association
171 of CK2 or 14-3-3 with Raf, further demonstrating their independence from Raf phospho-
172 rylation. Interestingly, the Raf-Akt interaction qualitatively increased following treatment
173 with GW5074; however, it remained unaffected by treatment with ATRA. Src family ki-
174 nases are known to be important in myeloid differentiation (23) and their role in HL-60

175 differentiation has been investigated elsewhere (11). Given the existing work and variable
176 reproducibility in the context of the Raf immunoprecipitate, we did not investigate the role
177 of Src further in this study. Taken together, the immunoprecipitation and GW5074 results
178 implicated Vav1 association to be correlated with Raf activation following ATRA-treatment.
179 Previous studies demonstrated that a Vav1-Slp76-Cbl-CD38 complex plays an important
180 role in ATRA-induced MAPK activation and differentiation of HL-60 cells (13). Here we
181 did not observe direct interaction of Raf with Cbl or Slp76; however, this complex could
182 be involved upstream.

183 Next, we considered the effect of the Raf kinase inhibitor GW5074 on functional mark-
184 ers of ATRA-induced growth arrest and differentiation. Inhibition of Raf kinase activity
185 modulated MAPK activation and differentiation markers following ATRA exposure (Fig.
186 5D-F). ATRA treatment alone statistically significantly increased the G1/G0 percentage
187 over the untreated control, while GW5074 alone had a negligible effect on the cell cycle
188 distribution (Fig. 5D). Surprisingly, the combination of GW5074 and ATRA statistically
189 significantly increased the G1/G0 population ($82 \pm 1\%$) compared with ATRA alone (61
190 $\pm 0.5\%$). Increased G1/G0 arrest following the combined treatment with GW5074 and
191 ATRA was unexpected, as the combination of ATRA and the MEK inhibitor (PD98059) has
192 been shown previously to decrease ATRA-induced growth arrest (8). However, growth ar-
193 rest is not the sole indication of functional differentiation. Expression of the cell surface
194 marker CD11b has also been shown to coincide with HL-60 cells myeloid differentiation
195 (24). We measured CD11b expression, for the various treatment groups, using immuno-
196 fluorescence flow cytometry 48 hr post-treatment. As with G1/G0 arrest, ATRA alone
197 increased CD11b expression over the untreated control, while GW5074 further enhanced
198 ATRA-induced CD11b expression (Fig. 5E). GW5074 alone had no statistically significant
199 effect on CD11b expression, compared with the untreated control. Lastly, the inducible re-
200 active oxygen species (ROS) response was used as a functional marker of differentiated

201 neutrophils (16). We measured the ROS response induced by the phorbol ester 12-O-
202 tetradecanoylphorbol-13-acetate (TPA) using flow cytometry. Untreated cells showed no
203 discernible TPA response, with only $7.0 \pm 3.0\%$ ROS induction (Fig. 5F). Cells treated
204 with ATRA had a significantly increased TPA response, $53 \pm 7\%$ ROS induction 48 hr
205 post-treatment. Treatment with both ATRA and GW5074 statistically significantly reduced
206 ROS induction ($22 \pm 0.6\%$) compared to ATRA alone. Interestingly, Western blot analy-
207 sis did not detect a GW5074 effect on ATRA-induced expression of p47phox, a required
208 upstream component of the ROS response (Fig. 5F, bottom). Thus, the inhibitory effect
209 of GW5074 on inducible ROS might occur downstream of p47phox expression. How-
210 ever, the ROS producing complex is MAPK dependent, therefore it is also possible that
211 GW5074 inhibited ROS production by interfering with MAPK activation (in which case the
212 p47Phox marker might not accurately reflect phenotypic conversion and differentiation).

213 **Discussion**

214 In this study, we presented an effective model of ATRA-inducible differentiation of HL-60
215 cells which encoded positive feedback between the ATRA-inducible signalsome complex
216 and the MAPK pathway. Despite its simplicity, the model captured key features of the
217 ATRA induced differentiation such as sustained MAPK activation, and bistability with re-
218 spect to ATRA exposure. We also reported a new ATRA-inducible component of the
219 signalsome, Vav1. Vav1 is a guanine nucleotide exchange factor for Rho family GTPases
220 that activate pathways leading to actin cytoskeletal rearrangements and transcriptional al-
221 terations (25). The Vav1/Raf association correlated with Raf activity, was ATRA-inducible
222 and decreased after treatment with GW5074. The presence of Vav1 in Raf/Grb2 com-
223 plexes has been shown to correlate with increased Raf activity in mast cells (26). Fur-
224 thermore, studies on Vav1 knockout mice demonstrated that the loss of Vav1 resulted
225 in deficiencies of ERK signaling for both T-cells as well as neutrophils (27, 28). While its
226 function in the signalsome is unclear, Vav1 has been shown to associate with a Cbl-Slp76-
227 CD38 complex in an ATRA-dependent manner; furthermore, transfection of HL-60 cells
228 with Cbl mutants that fail to bind CD38, yet still bind Slp76 and Vav1, prevented ATRA-
229 induced MAPK activation (13). Thus, interaction of Cbl-Slp76-Vav1 and CD38 appears to
230 be required for transmission of the ATRA signal by the signalsome.

231 We conducted immunoprecipitation studies and identified a limited number of ATRA-
232 dependent and -independent Raf interaction partners. While we were unable to detect
233 the association of Raf with common kinases and GTPases such as PKC, PKA, p38, Rac
234 and Rho, we did establish potential interactions between Raf and key partners such as
235 Vav1, Src, Akt, CK2 and 14-3-3. All of these partners are known to be associated with Raf
236 activation or function. Src is known to bind Raf through an SH2 domain, and this associ-
237 ation has been shown to be dependent of the serine phosphorylation of Raf (29). Thus,
238 an ATRA inducible Src/Raf association may be a result of ATRA-induced Raf phospho-

239 phosphorylation at S259 or S621. We also identified an interaction between Raf and the Ser/Thr
240 kinases Akt and CK2. Akt can phosphorylate Raf at S259, as demonstrated by studies
241 in a human breast cancer line (30). CK2 can also phosphorylate Raf, although the lit-
242 erature has traditionally focused on S338 and not S621 or S259(31). However, neither
243 of these kinase interactions were ATRA-inducible, suggesting their association with Raf
244 alone was not associated with ATRA-induced Raf phosphorylation. The adapter protein
245 14-3-3 was also constitutively associated with Raf. The interaction between Raf and 14-
246 3-3 has been associated with both S621 and S259 phosphorylation and activity (32).
247 Additionally, the association of Raf with 14-3-3 not only stabilized S621 phosphorylation,
248 but also reversed the S621 phosphorylation from inhibitory to activating (33). Finally, we
249 found that Vav1/Raf association correlated with Raf activity, was ATRA-inducible and de-
250 creased after treatment with GW5074. The presence of Vav1 in Raf/Grb2 complexes has
251 been shown to correlate with increased Raf activity in mast cells (26). Furthermore, stud-
252 ies on Vav1 knockout mice demonstrated that the loss of Vav1 resulted in deficiencies of
253 ERK signaling for both T-cells as well as neutrophils (27, 28). Interestingly, while an in-
254 tegrin ligand-induced ROS response was blocked in Vav1 knockout neutrophils, TPA was
255 able to bypass the Vav1 requirement and stimulate both ERK phosphorylation and ROS
256 induction (28). In this study, the TPA-induced ROS response was dependent upon Raf
257 kinase activity, and was mitigated by the addition of GW5074. It is possible that Vav1 is
258 downstream of various integrin receptors but upstream of Raf in terms of inducible ROS
259 responses. Vav1 has also been shown to associate with a Cbl-Slp76-CD38 complex in an
260 ATRA-dependent manner; furthermore, transfection of HL-60 cells with Cbl mutants that
261 fail to bind CD38, yet still bind Slp76 and Vav1, prevents ATRA-induced MAPK activation
262 (13). The literature suggest a variety of possible receptor-signaling pathways, which in-
263 volve Vav1, for MAPK activation; moreover, given the ATRA-inducible association Vav1
264 may play a direct role in Raf activation.

265 We hypothesized that Vav1 is a member of an ATRA-inducible complex which propels
266 sustained MAPK activation, arrest and differentiation. Initially, ATRA-induced Vav1 ex-
267 pression drives increased association between Vav1 and Raf. This increased interaction
268 facilitates phosphorylation and activation of Raf by pre-bound Akt and/or CK2 at S621
269 or perhaps S259. Constitutively bound 14-3-3 may also stabilize the S621 phosphory-
270 lation, modulate the activity and/or up-regulate autophosphorylation. Activated Raf can
271 then drive ERK activation, which in turn closes the positive feedback loop by activating
272 Raf transcription factors, e.g. Sp1 and/or STAT1 (34–37). We tested this working hy-
273 pothesis using mathematical modeling. The model recapitulated both ATRA time-course
274 data as well as the GW5074 inhibitor effects. This suggested the proposed Raf-Vav1
275 architecture was at least consistent with the experimental studies. Further, analysis of
276 the Raf-Vav1 model identified bistability in ppERK levels. Thus, two possible MAPK ac-
277 tivation branches were possible for experimentally testable ATRA values. The analysis
278 also suggested the ATRA-induced Raf-Vav1 architecture could be locked into a sustained
279 signaling mode (high ppERK) even in the absence of a ATRA signal. This locked-in prop-
280 erty could give rise to an ATRA-induction memory. We validated the treatment memory
281 property predicted by the Raf-Vav1 circuit experimentally using ATRA-washout experi-
282 ments. ERK phosphorylation levels remained high for more then 96 hr after ATRA was
283 removed. Previous studies demonstrated that HL-60 cells possessed an inheritable mem-
284 ory of ATRA stimulus (38). Although the active state was self-sustaining, the inactive state
285 demonstrated considerable robustness to perturbation. For example, we found that 50x
286 overexpression of Raf was required to reliably lock MAPK into the activated state, while
287 small perturbations had almost no effect on ppERK levels over the entire ensemble. CD38
288 expression correlated with the ppERK, suggesting its involvement in the signaling com-
289 plex. Our computational and experimental results showed that positive feedback, through
290 ERK-dependent Raf expression, could sustain MAPK signaling through many division cy-

291 cles. Such molecular mechanisms could underly aspects of cellular memory associated
292 to consecutive ATRA treatments.

293 Several engineered, or naturally occurring systems involved in cell fate decisions incor-
294 porate positive feedback and bistability (39). One of the most well studied cell fate circuits
295 is the Mos mitogen-activated protein kinase cascade in *Xenopus* oocytes. This cascade
296 is activated when oocytes are induced by the steroid hormone progesterone (40). The
297 MEK-dependent activation of p42 MAPK stimulates the accumulation of the Mos onco-
298 protein, which in turn activates MEK, thereby closing the feedback loop. This is similar to
299 the differentiation circuit presented here; ATRA drives signalsome which activates MAPK,
300 cell-cycle arrest, differentiation and signalsome. Thus, while HL-60 and *Xenopus* oocytes
301 are vastly different biological models, they share similar cell fate decision architectures.
302 Other unrelated cell fate decisions such as programmed cell death have also been sug-
303 gested to be bistable (41). Still more biochemical networks important to human health,
304 for example the human coagulation or complement cascades, also feature strong positive
305 feedback elements (42). Thus, while positive feedback is sometimes not desirable in man-
306 made systems, it may be at the core of a diverse variety of cell fate programs and other
307 networks important to human health.

308 Model performance was impressive given its limited size. However, there were several
309 issues to explore further. First, there was likely missing connectivity in the effective differ-
310 entiation circuit. Decreasing BLR1 expression with simultaneously sustained cRaf-pS261
311 activation was not captured by the current network architecture. This suggested that
312 signalsome, once activated, had a long lifetime as decreased BLR1 expression did not
313 impact cRaf-pS261 abundance. We could model this by separating signalsome formation
314 into an inactive precursor pool that is transformed to a long-lived activated signalsome by
315 MAPK activation. We should also explore adding additional downstream biological mod-
316 ules to this skeleton model, for example the upregulation of reactive oxygen markers such

317 as p47Phox or cell cycle arrest components to capture the switch from an actively prolif-
318 erating population to a population in G0-arrest. Next, the choice of max/min integration
319 rules or the particular form of the transfer functions could also be explored. Integration
320 rules other than max/min could be used, such as the mean or the product, assuming the
321 range of the transfer functions is always $f \in [0, 1]$. Alternative integration rules might
322 have different properties which could influence model identification or performance. For
323 example, a mean integration rule would be differentiable, allowing derivative-based opti-
324 mization approaches to be used. The form of the transfer function could also be explored.
325 We choose hill-like functions because of their prominence in the systems and synthetic
326 biology community. However, many other transfer functions are possible.

327 **Materials and Methods**

328 *Model equations.* We decomposed the ATRA-induced differentiation program into three
329 modules; a signal initiation module that sensed and transformed the ATRA signal into
330 activated cRaf-pS621 and the ATRA-RXR/RAR (activated Trigger) signals; a signal in-
331 tegration module that controlled the expression of upstream transcription factors given
332 cRaf-pS621 and activated Trigger signals; and a phenotype module which encoded the
333 expression of functional differentiation markers from the ATRA-inducible transcription fac-
334 tors. The output of the signal initiation module was the input to the gene expression
335 model. For each gene $j = 1, 2, \dots, \mathcal{G}$, we modeled both the mRNA (m_j) and protein (p_j)
336 abundance:

$$\frac{dm_j}{dt} = r_{T,j} - (\mu + \theta_{m,j}) m_j + \lambda_j \quad (1)$$

$$\frac{dp_j}{dt} = r_{X,j} - (\mu + \theta_{p,j}) p_j \quad (2)$$

337 The terms $r_{T,j}$ and $r_{X,j}$ denote the specific rates of transcription, and translation while
338 the terms $\theta_{m,j}$ and $\theta_{p,j}$ denote first-order degradation constants for mRNA and protein,
339 respectively. The specific transcription rate $r_{T,j}$ was modeled as the product of a kinetic
340 term $\bar{r}_{T,j}$ and a control term u_j which described how the abundance of transcription fac-
341 tors, or other regulators influenced the expression of gene j . The kinetic transcription
342 term $\bar{r}_{T,j}$ was modeled as:

$$\bar{r}_{T,j} = V_T^{max} \left(\frac{L_{T,o}}{L_{T,j}} \right) \left(\frac{G_j}{K_T + G_j} \right) \quad (3)$$

343 where the maximum gene expression rate V_T^{max} was defined as the product of a char-
344 acteristic transcription rate constant (k_T) and the abundance of RNA polymerase (R_1),
345 $V_T^{max} = k_T (R_1)$. The $(L_{T,o}/L_{T,j})$ term denotes the ratio of transcription read lengths; $L_{T,o}$

346 represents a characteristic gene length, while $L_{T,j}$ denotes the length of gene j . Thus,
 347 the ratio $(L_{T,o}/L_{T,j})$ is a gene specific correction to the characteristic transcription rate
 348 V_T^{max} . The degradation rate constants were defined as $\theta_{m,j}$ and $\theta_{p,j}$ denote characteristic
 349 degradation constants for mRNA and protein, respectively. Lastly, the λ_j term denotes the
 350 constitutive rate of expression of gene j .

351 The gene expression control term $0 \leq u_j \leq 1$ depended upon the combination of fac-
 352 tors which influenced the expression of gene j . If the expression of gene j was influenced
 353 by $1, \dots, m$ factors, we modeled this relationship as $u_j = \mathcal{I}_j(f_{1j}(\cdot), \dots, f_{mj}(\cdot))$ where
 354 $0 \leq f_{ij}(\cdot) \leq 1$ denotes a regulatory transfer function quantifying the influence of factor i
 355 on the expression of gene j , and $\mathcal{I}_j(\cdot)$ denotes an integration rule which combines the
 356 individual regulatory inputs for gene j into a single control term. In this study, the integra-
 357 tion rule governing gene expression was the weighted fraction of promoter configurations
 358 that resulted in gene expression [REFHERE]:

$$u_j = \frac{W_{R_{1,j}} + \sum_n W_{nj} f_{nj}}{1 + W_{R_{1,j}} + \sum_d W_{dj} f_{dj}} \quad (4)$$

359 The numerator, the weighted sum (with weights W_{nj}) of promoter configurations leading to
 360 gene expression, was normalized by all possible promoter configurations. The likelihood
 361 of each configuration was quantified by the transfer function f_{nj} (which we modeled using
 362 hill like functions), while the lead term in the numerator $W_{R_{1,j}}$ denotes the weight of con-
 363 stitutive expression for gene j . Given this formulation, the rate of constitutive expression
 364 was then given by:

$$\lambda_j = \bar{r}_{T,j} \left(\frac{W_{R_{1,j}}}{1 + W_{R_{1,j}}} \right) \quad (5)$$

365 If a gene expression process had no modifying factors, $u_j = 1$. Lastly, the specific trans-

366 lation rate was modeled as:

$$r_{X,j} = V_X^{\max} \left(\frac{L_{X,o}}{L_{X,j}} \right) \left(\frac{m_j}{K_X + m_j} \right) \quad (6)$$

367 where V_X^{\max} denotes a characteristic maximum translation rate estimated from literature,
368 and K_X denotes a translation saturation constant. The characteristic maximum translation
369 rate was defined as the product of a characteristic translation rate constant (k_X) and
370 the Ribosome abundance (R_2), $V_X^{\max} = k_X (R_2)$. As was the case for transcription, we
371 corrected the characteristic translation rate by the ratio of the length of a characteristic
372 transcription normalized by the length of transcript j .

373 The signal initiation, and integration modules required the level of cRaf-pS621 and
374 ATRA-RXR/RAR (activated Trigger) as inputs. However, our base model described only
375 the abundance of inactive proteins e.g., cRaf or RXR/RAR but not the activated forms.
376 To address this issue, we estimated pseudo steady state approximations for the abun-
377 dance of cRaf-pS621 and activated Trigger. The abundance of activated trigger ($x_{a,1}$) was
378 estimated directly from the RXR/RAR abundance ($x_{u,1}$):

$$x_{a,1} \sim x_{u,1} \left(\frac{\alpha \times \text{ATRA}}{1 + \alpha \times \text{ATRA}} \right) \quad (7)$$

379 On the other hand, the abundance of cRaf-pS621 was estimated by making the pseudo
380 steady state approximation on the cRaf-pS621 balance. The abundance of an activated
381 signaling species i was given by:

$$\frac{dx_i}{dt} = r_{+,i}(\mathbf{x}, \mathbf{k}) - (\mu + k_{d,i}) x_i \quad i = 1, \dots, \mathcal{M} \quad (8)$$

382 The quantity x_i denotes concentration of signaling species i , while \mathcal{R} and \mathcal{M} denote
383 the number of signaling reactions and signaling species in the model, respectively. The

384 term $r_{+,i}(\mathbf{x}, \mathbf{k})$ denotes the rate of generation of activated species i , while μ denotes the
 385 specific growth rate, and $k_{d,i}$ denotes the rate constant controlling the non-specific degra-
 386 dation of x_i . We have neglected deactivation reactions e.g., phosphatase activities. We
 387 assumed that signaling processes were fast compared to gene expression; this allowed
 388 us to approximate the signaling balance as:

$$x_i^* \simeq \frac{r_{+,i}(\mathbf{x}, \mathbf{k})}{(\mu + k_{d,i})} \quad i = 1, \dots, \mathcal{M} \quad (9)$$

389 The generation rate was written as the product of a kinetic term ($\bar{r}_{+,i}$) and a control term
 390 (v_i). The control terms $0 \leq v_j \leq 1$ depended upon the combination of factors which in-
 391 fluenced rate process j . If rate j was influenced by $1, \dots, m$ factors, we modeled this
 392 relationship as $v_j = \mathcal{I}_j(f_{1j}(\cdot), \dots, f_{mj}(\cdot))$ where $0 \leq f_{ij}(\cdot) \leq 1$ denotes a regulatory
 393 transfer function quantifying the influence of factor i on rate j . The function $\mathcal{I}_j(\cdot)$ is an
 394 integration rule which maps the output of regulatory transfer functions into a control vari-
 395 able. In this study, we used $\mathcal{I}_j \in \{\min, \max\}$ and hill transfer functions (43). If a process
 396 had no modifying factors, $v_j = 1$. The kinetic rate of cRaf-pS621 generation $\bar{r}_{+,cRaf}$ was
 397 given as:

$$\bar{r}_{+,cRaf} = k_{+,cRaf} x_s \left(\frac{x_{cRaf}}{K_{+,cRaf} + x_{cRaf}} \right) \quad (10)$$

398 where x_s denotes the signalsome abundance, and $K_{+,cRaf}$ denotes a saturation constant
 399 governing cRaf-pS621 formation. The formation of cRaf-pS621 was regulated by a single
 400 factor, the abundance of MAPK inhibitor, thus $v_{+,cRaf}$ took the form:

$$v_{+,cRaf} = \left(1 - \frac{I}{K_D + I} \right) \quad (11)$$

401 where I denotes the MAPK inhibitor abundance, and K_D the affinity constant for inhibitor
 402 I .

403 *Estimation of signaling and gene expression model parameters.* We estimated the W_{ij}
 404 parameters, and the parameters in the transfer functions f_{d_j} from gene expression data
 405 sets. On the other hand, we estimated $k_T, k_X, \theta_{m,j}, \theta_{p,j}, R_1$ and R_2 using estimates of
 406 transcription and translation rates, the half-life of a typical mRNA and protein, and a typ-
 407 ical value for the copies per cell of RNA polymerase and ribosomes from literature (44).
 408 The saturation constants K_X and K_T were adjusted so that gene expression and trans-
 409 lation resulted in gene products on a biologically realistic concentration scale. Lastly, we
 410 calculated the concentration for gene G_j by assuming, on average, that a cell had two
 411 copies of each gene at any given time. Thus, the bulk of our gene expression param-
 412 eters were based directly upon literature values, and were not adjusted during model
 413 identification. The values used for the characteristic transcription/translation parameters,
 414 degradation constants and macromolecular copy number are given in the supplemental
 415 materials along with the specific formulas required to calculate all derived constants.

416 Signal and gene expression model parameters were estimated by minimizing the
 417 squared difference between simulations and experimental data set j :

$$E_j(\mathbf{k}) = \sum_{i=1}^{\mathcal{T}_j} \left(\hat{\mathcal{M}}_{ij} - \hat{y}_{ij}(\mathbf{k}) \right)^2 + \left(\frac{\mathcal{M}'_{ij} - \max y_{ij}}{\mathcal{M}'_{ij}} \right)^2 \quad (12)$$

418 The terms $\hat{\mathcal{M}}_{ij}$ and \hat{y}_{ij} denote scaled experimental observations and simulation outputs
 419 at time i from training set j , where \mathcal{T}_j denoted the number of time points for data set j .
 420 The first term in Eqn. (12) quantified the relative simulation error. We used immunoblot
 421 intensity measurements for model training. Thus, we trained the model on the *relative*
 422 change between bands within each data set. Suppose we have the intensity of species x
 423 at time $\{t_1, t_2, \dots, t_n\}$ in condition j . The scaled value $0 \leq \hat{\mathcal{M}}_{ij} \leq 1$ is given by:

$$\hat{\mathcal{M}}_{ij} = \left(\mathcal{M}_{ij} - \min_i \mathcal{M}_{ij} \right) / \left(\max_i \mathcal{M}_{ij} - \min_i \mathcal{M}_{ij} \right) \quad (13)$$

424 where $\hat{M}_{ij} = 0$ and $\hat{M}_{ij} = 1$ describe the lowest (highest) intensity bands. A similar
425 scaling was used for the simulation output. The second term in the objective function
426 ensured a realistic concentration scale was estimated by the model. We set the highest
427 intensity band to $M'_{ij} = 10$ [AU] for all simulations. We minimized the total model residual
428 $\sum_j E_j$ using heuristic optimization starting from a random initial parameter guess.

429 The signaling and gene expression model equations were implemented in the Julia
430 programming language, and solved using the CVODE routine of the Sundials package (45,
431 46). The model code and parameter ensemble is freely available under an MIT software
432 license and can be downloaded from <http://www.varnerlab.org>.

433 *Cell culture and treatment* Human myeloblastic leukemia cells (HL-60 cells) were grown
434 in a humidified atmosphere of 5% CO₂ at 37°C and maintained in RPMI 1640 from Gibco
435 (Carlsbad, CA) supplemented with 5% heat inactivated fetal bovine serum from Hyclone
436 (Logan, UT) and 1× antibiotic/antimicotic (Gibco, Carlsbad, CA). Cells were cultured in
437 constant exponential growth (47). Experimental cultures were initiated at 0.1×10^6 cells/mL
438 24 hr prior to ATRA treatment; if indicated, cells were also treated with GW5074 (2 μ M) 18
439 hr before ATRA treatment. For the cell culture washout experiments, cells were treated
440 with ATRA for 24 hr, washed 3x with prewarmed serum supplemented culture medium
441 to remove ATRA, and reseeded in ATRA-free media as described. Western blot analysis
442 was performed at incremental time points after removal of ATRA.

443 *Chemicals* All-Trans Retinoic Acid (ATRA) from Sigma-Aldrich (St. Louis, MO) was dis-
444 solved in 100% ethanol with a stock concentration of 5mM, and used at a final concen-
445 tration of 1 μ M (unless otherwise noted). The cRaf inhibitor GW5074 from Sigma-Aldrich
446 (St. Louis, MO) was dissolved in DMSO with a stock concentration of 10mM, and used
447 at a final concentration of 2 μ M. HL-60 cells were treated with 2 μ M GW5074 with or with-
448 out ATRA (1 μ M) at 0 hr. This GW5074 dosage had a negligible effect on the cell cycle
449 distribution, compared to ATRA treatment alone.

450 *Immunoprecipitation and western blotting* Approximately 1.2×10^7 cells were lysed using
451 $400\mu\text{L}$ of M-Per lysis buffer from Thermo Scientific (Waltham, MA). Lysates were cleared
452 by centrifugation at $16,950 \times g$ in a micro-centrifuge for 20 min at 4°C . Lysates were
453 pre-cleared using $100\mu\text{L}$ protein A/G Plus agarose beads from Santa Cruz Biotechnology
454 (Santa Cruz, CA) by inverting overnight at 4°C . Beads were cleared by centrifugation and
455 total protein concentration was determined by a BCA assay (Thermo Scientific, Waltham,
456 MA). Immunoprecipitations were setup by bringing lysate to a concentration of 1g/L in a
457 total volume of $300\mu\text{L}$ (M-Per buffer was used for dilution). The anti-Raf antibody was
458 added at $3\mu\text{L}$. A negative control with no bait protein was also used to exclude the di-
459 rect interaction of proteins with the A/G beads. After 1 hr of inversion at 4°C , $20\mu\text{L}$ of
460 agarose beads was added and samples were left to invert overnight at 4°C . Samples
461 were then washed three times with M-Per buffer by centrifugation. Finally proteins were
462 eluted from agarose beads using a laemmli loading buffer. Eluted proteins were resolved
463 by SDS-PAGE and Western blotting. Total lysate samples were normalized by total protein
464 concentration ($20\mu\text{g}$ per sample) and resolved by SDS-PAGE and Western blotting. Sec-
465 ondary HRP bound antibody was used for visualization. All antibodies were purchased
466 from Cell Signaling (Boston, MA) with the exception of α -p621 Raf which was purchased
467 from Biosource/Invitrogen (Carlsbad, CA), and α -CK2 from BD Biosciences (San Jose,
468 CA).

469 *Morphology assessment* Untreated and ATRA-treated HL-60 cells were collected after
470 72 hr and cytocentrifuged for 3 min at 700 rpm onto glass slides. Slides were air-dried
471 and stained with Wright's stain. Slide images were captured at 40X (Leica DM LB 100T
472 microscope, Leica Microsystems).

473 **Competing interests**

474 The authors declare that they have no competing interests.

475 **Author's contributions**

476 J.V and A.Y directed the study. R.T, H.J and J.C conducted the cell culture measure-
477 ments. J.V and W.D developed the reduced order HL-60 models and the parameter en-
478 semble. W.D analyzed the model ensemble, and generated figures for the manuscript.
479 The manuscript was prepared and edited for publication by W.D, A.Y and J.V.

480 **Acknowledgements**

481 We gratefully acknowledge the suggestions from the anonymous reviewers to improve
482 this manuscript.

483 **Funding**

484 We acknowledge the financial support to J.V. by the National Science Foundation CA-
485 REER (CBET-0846876) for the support of R.T. and H.J. In addition, we acknowledge
486 support to A.Y. from the National Institutes of Health (CA 30555, CA152870) and a grant
487 from New York State Stem Cell Science. Lastly, we acknowledge the financial support to
488 J.V. and A.Y. from the National Cancer Institute (#U54 CA143876). The content is solely
489 the responsibility of the authors and does not necessarily represent the official views of
490 the National Cancer Institute or the National Institutes of Health.

491 **References**

- 492 1. Bushue N, Wan YJY (2010) Retinoid pathway and cancer therapeutics. *Adv Drug
493 Deliv Rev* 62: 1285-98.
- 494 2. Tang XH, Gudas LJ (2011) Retinoids, retinoic acid receptors, and cancer. *Annu Rev
495 Pathol* 6: 345-64.
- 496 3. Cheung FSG, Lovicu FJ, Reichardt JKV (2012) Current progress in using vitamin d
497 and its analogs for cancer prevention and treatment. *Expert Rev Anticancer Ther* 12:
498 811-37.
- 499 4. Nilsson B (1984) Probable in vivo induction of differentiation by retinoic acid of
500 promyelocytes in acute promyelocytic leukaemia. *Br J Haematol* 57: 365-71.
- 501 5. Warrell RP Jr (1993) Retinoid resistance in acute promyelocytic leukemia: new mech-
502 anisms, strategies, and implications. *Blood* 82: 1949-53.
- 503 6. Freemantle SJ, Spinella MJ, Dmitrovsky E (2003) Retinoids in cancer therapy and
504 chemoprevention: promise meets resistance. *Oncogene* 22: 7305-15.
- 505 7. Breitman TR, Selonick SE, Collins SJ (1980) Induction of differentiation of the human
506 promyelocytic leukemia cell line (HL-60) by retinoic acid. *Proc Natl Acad Sci U S A*
507 77: 2936–2940.
- 508 8. Yen A, Roberson MS, Varvayanis S, Lee AT (1998) Retinoic acid induced
509 mitogen-activated protein (MAP)/extracellular signal-regulated kinase (ERK) kinase-
510 dependent MAP kinase activation needed to elicit HL-60 cell differentiation and
511 growth arrest. *Cancer Res* 58: 3163–3172.
- 512 9. Hong HY, Varvayanis S, Yen A (2001) Retinoic acid causes MEK-dependent RAF
513 phosphorylation through RARalpha plus RXR activation in HL-60 cells. *Differentiation*
514 68: 55–66.
- 515 10. Mangelsdorf DJ, Ong ES, Dyck JA, Evans RM (1990) Nuclear receptor that identifies
516 a novel retinoic acid response pathway. *Nature* 345: 224–229.

- 517 11. Congleton J, MacDonald R, Yen A (2012) Src inhibitors, PP2 and dasatinib, increase
518 retinoic acid-induced association of Lyn and c-Raf (S259) and enhance MAPK-
519 dependent differentiation of myeloid leukemia cells. Leukemia 26: 1180-8.
- 520 12. Shen M, Bunaci R, Congleton J, Jensen H, Sayam L, et al. (2011) Interferon regula-
521 tory factor-1 binds c-Cbl, enhances mitogen activated protein kinase signaling and
522 promotes retinoic acid-induced differentiation of HL-60 human myelo-monoblastic
523 leukemia cells. Leuk Lymphoma 52: 2372-9.
- 524 13. Shen M, Yen A (2009) c-Cbl tyrosine kinase-binding domain mutant G306E abolishes
525 the interaction of c-Cbl with CD38 and fails to promote retinoic acid-induced cell dif-
526 ferentiation and G0 arrest. J Biol Chem 284: 25664–25677.
- 527 14. Yen A, Varvayanis S, Smith J, Lamkin T (2006) Retinoic acid induces expression of
528 SLP-76: expression with c-FMS enhances ERK activation and retinoic acid-induced
529 differentiation/G0 arrest of HL-60 cells. Eur J Cell Biol 85: 117–132.
- 530 15. Marchisio M, Bertagnolo V, Colamussi ML, Capitani S, Neri LM (1998) Phosphatidyli-
531 nositol 3-kinase in HL-60 nuclei is bound to the nuclear matrix and increases during
532 granulocytic differentiation. Biochem Biophys Res Commun 253: 346-51.
- 533 16. Congleton J, Jiang H, Malavasi F, Lin H, Yen A (2011) ATRA-induced HL-60 myeloid
534 leukemia cell differentiation depends on the CD38 cytosolic tail needed for membrane
535 localization, but CD38 enzymatic activity is unnecessary. Exp Cell Res 317: 910–
536 919.
- 537 17. Wang J, Yen A (2004) A novel retinoic acid-responsive element regulates retinoic acid
538 induced BLR1 expression. Mol Cell Biol 24: 2423 - 2443.
- 539 18. Yen A (1990) HL-60 cells as a model of growth and differentiation: the significance of
540 variant cells. Hematology Review 4: 5-46.
- 541 19. Yang T, Xiong Q, Enslen H, Davis R, Chow CW (2002) Phosphorylation of NFATc4 by
542 p38 mitogen-activated protein kinases. Mol Cell Biol 22: 3892–3904.

- 543 20. Wang J, Yen A (2008) A MAPK-positive Feedback Mechanism for BLR1 Signaling
544 Propels Retinoic Acid-triggered Differentiation and Cell Cycle Arrest. *J Biol Chem*
545 283: 4375–4386.
- 546 21. Tasseff R, Nayak S, Song S, Yen A, Varner J (2011) Modeling and analysis of retinoic
547 acid induced differentiation of uncommitted precursor cells. *Integr Biol* 3: 578 - 591.
- 548 22. Katagiri K, Hattori S, Nakamura S, Yamamoto T, Yoshida T, et al. (1994) Activation
549 of ras and formation of gap complex during tpa-induced monocytic differentiation of
550 hl-60 cells. *Blood* 84: 1780–1789.
- 551 23. Miranda MB, Johnson DE (2007) Signal transduction pathways that contribute to
552 myeloid differentiation. *Leukemia* 21: 1363–1377.
- 553 24. Hickstein DD, Back AL, Collins SJ (1989) Regulation of expression of the cd11b and
554 cd18 subunits of the neutrophil adherence receptor during human myeloid differenti-
555 ation. *J Biol Chem* 264: 21812–21817.
- 556 25. Hornstein I, Alcover A, Katzav S (2004) Vav proteins, masters of the world of cy-
557 toskeleton organization. *Cell Signal* 16: 1-11.
- 558 26. Song JS, Gomez J, Stancato LF, Rivera J (1996) Association of a p95 vav-containing
559 signaling complex with the fcepsilonlonri gamma chain in the rbl-2h3 mast cell line. ev-
560 idence for a constitutive in vivo association of vav with grb2, raf-1, and erk2 in an
561 active complex. *J Biol Chem* 271: 26962–26970.
- 562 27. Costello PS, Walters AE, Mee PJ, Turner M, Reynolds LF, et al. (1999) The rho-family
563 gtp exchange factor vav is a critical transducer of t cell receptor signals to the calcium,
564 erk, and nf-kappab pathways. *Proc Natl Acad Sci U S A* 96: 3035–3040.
- 565 28. Graham D, Robertson C, Bautista J, Mascarenhas F, Diacovo M, et al. (2007)
566 Neutrophil-mediated oxidative burst and host defense are controlled by a Vav-
567 PLCgamma2 signaling axis in mice. *J Clin Invest* 117: 3445–3452.
- 568 29. Cleghon V, Morrison DK (1994) Raf-1 interacts with fyn and src in a non-

- 569 phosphotyrosine-dependent manner. *J Biol Chem* 269: 17749–17755.
- 570 30. Zimmermann S, Moelling K (1999) Phosphorylation and regulation of raf by akt (pro-
571 tein kinase b). *Science* 286: 1741–1744.
- 572 31. Ritt DA, Zhou M, Conrads TP, Veenstra TD, Copeland TD, et al. (2007) Ck2 is a
573 component of the ksr1 scaffold complex that contributes to raf kinase activation. *Curr
574 Biol* 17: 179–184.
- 575 32. Hekman M, Wiese S, Metz R, Albert S, Troppmair J, et al. (2004) Dynamic changes in
576 c-raf phosphorylation and 14-3-3 protein binding in response to growth factor stimula-
577 tion: differential roles of 14-3-3 protein binding sites. *J Biol Chem* 279: 14074–14086.
- 578 33. Dhillon AS, Yip YY, Grindlay GJ, Pakay JL, Dangers M, et al. (2009) The c-terminus
579 of raf-1 acts as a 14-3-3-dependent activation switch. *Cell Signal* 21: 1645–1651.
- 580 34. Kim HS, Lim IK (2009) Phosphorylated extracellular signal-regulated protein kinases
581 1 and 2 phosphorylate sp1 on serine 59 and regulate cellular senescence via tran-
582 scription of p21sdi1/cip1/waf1. *J Biol Chem* 284: 15475–15486.
- 583 35. Milanini-Mongiat J, Pouyss?gur J, Pag?as G (2002) Identification of two sp1 phospho-
584 rylation sites for p42/p44 mitogen-activated protein kinases: their implication in vas-
585 cular endothelial growth factor gene transcription. *J Biol Chem* 277: 20631–20639.
- 586 36. Zhang Y, Cho YY, Petersen BL, Zhu F, Dong Z (2004) Evidence of stat1 phospho-
587 lation modulated by mapks, mek1 and msk1. *Carcinogenesis* 25: 1165–1175.
- 588 37. Li Z, Theus MH, Wei L (2006) Role of erk 1/2 signaling in neuronal differentiation of
589 cultured embryonic stem cells. *Dev Growth Differ* 48: 513–523.
- 590 38. Yen A, Reece SL, Albright KL (1984) Dependence of hl-60 myeloid cell differentiation
591 on continuous and split retinoic acid exposures: precommitment memory associated
592 with altered nuclear structure. *J Cell Physiol* 118: 277–286.
- 593 39. Ferrell J (2002) Self-perpetuating states in signal transduction: positive feedback,
594 double-negative feedback and bistability. *Curr Opin Cell Biol* 14: 140-8.

- 595 40. Xiong W, Ferrell J (2003) A positive-feedback-based bistable 'memory module' that
596 governs a cell fate decision. *Nature* 426: 460-5.
- 597 41. Bagci EZ, Vodovotz Y, Billiar TR, Ermentrout GB, Bahar I (2006) Bistability in apop-
598 tosis: roles of bax, bcl-2, and mitochondrial permeability transition pores. *Biophys J*
599 90: 1546-59.
- 600 42. Luan D, Zai M, Varner JD (2007) Computationally derived points of fragility of a human
601 cascade are consistent with current therapeutic strategies. *PLoS Comput Biol* 3:
602 e142.
- 603 43. Wayman JA, Sagar A, Varner JD (2015) Dynamic modeling of cell-free biochemical
604 networks using effective kinetic models. *Processes* 3: 138.
- 605 44. Milo R, Jorgensen P, Moran U, Weber G, Springer M (2010) Bionumbers—the
606 database of key numbers in molecular and cell biology. *Nucleic Acids Res* 38: D750-
607 3.
- 608 45. Bezanson J, Edelman A, Karpinski S, Shah VB (2014) Julia: A fresh approach to
609 numerical computing. *CoRR* abs/1411.1607.
- 610 46. Hindmarsh A, Brown P, Grant K, Lee S, Serban R, et al. (2005) Sundials: Suite of non-
611 linear and differential/algebraic equation solvers. *ACM Transactions on Mathematical
612 Software* 31: 363-396.
- 613 47. Brooks SC, Kazmer S, Levin AA, Yen A (1996) Myeloid differentiation and retinoblas-
614 toma phosphorylation changes in HL-60 cells induced by retinoic acid receptor- and
615 retinoid X receptor-selective retinoic acid analogs. *Blood* 87: 227–237.
- 616 48. Jensen HA, Yourish HB, Bunaciu RP, Varner JD, Yen A (2015) Induced myelomono-
617 cytic differentiation in leukemia cells is accompanied by noncanonical transcription
618 factor expression. *FEBS Open Bio* 5: 789-800.

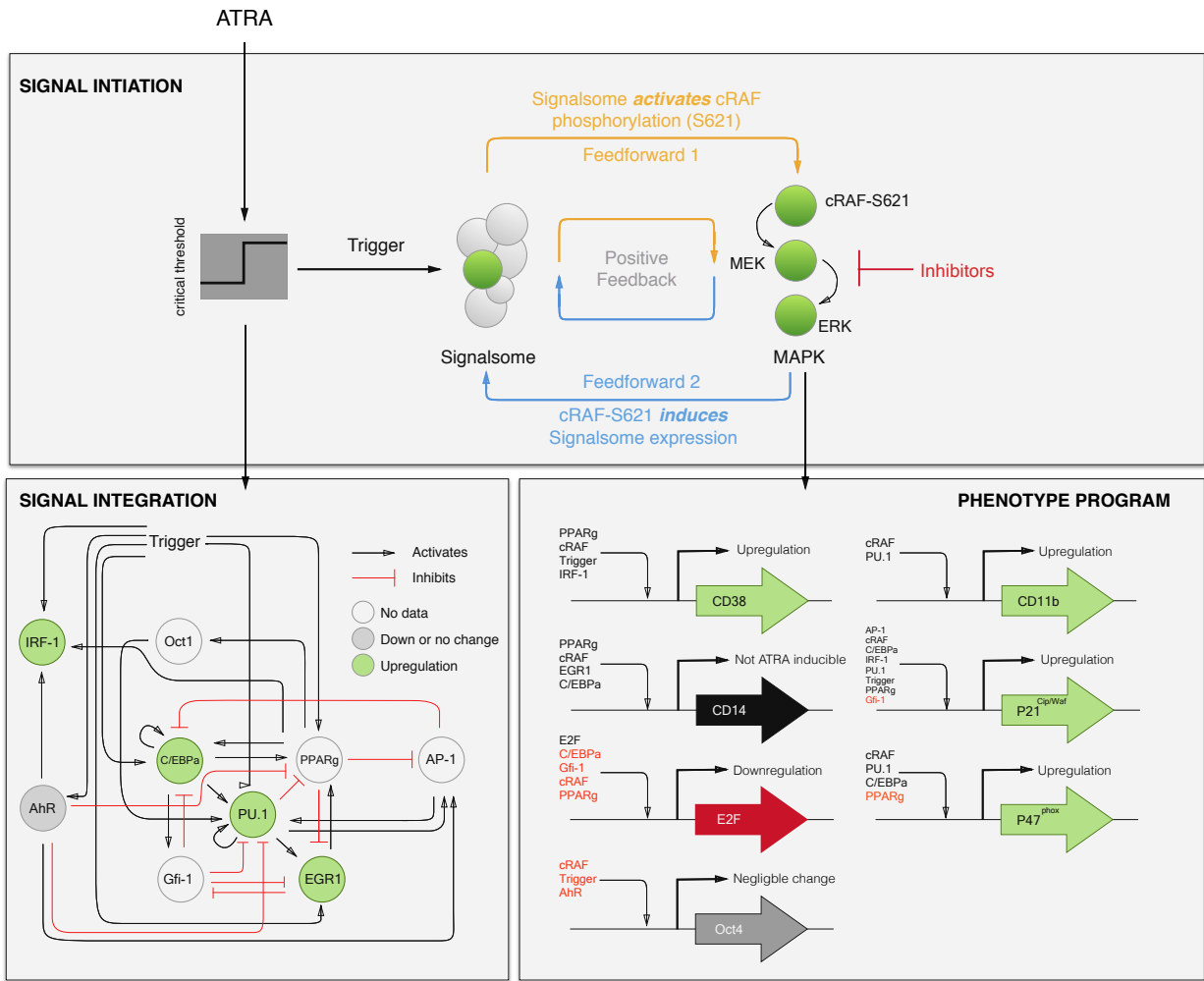


Fig. 1: Schematic of the effective ATRA differentiation circuit. Above a critical threshold, ATRA activates an upstream Trigger, which induces signalsome complex formation. Signalsome activates the mitogen-activated protein kinase (MAPK) cascade which in turn drives the differentiation program and signalsome formation. Both Trigger and activated cRaf-pS621 drive a phenotype gene expression program responsible for differentiation. Trigger activates the expression of a series of transcription factors which in combination with cRaf-pS621 result in phenotypic change.

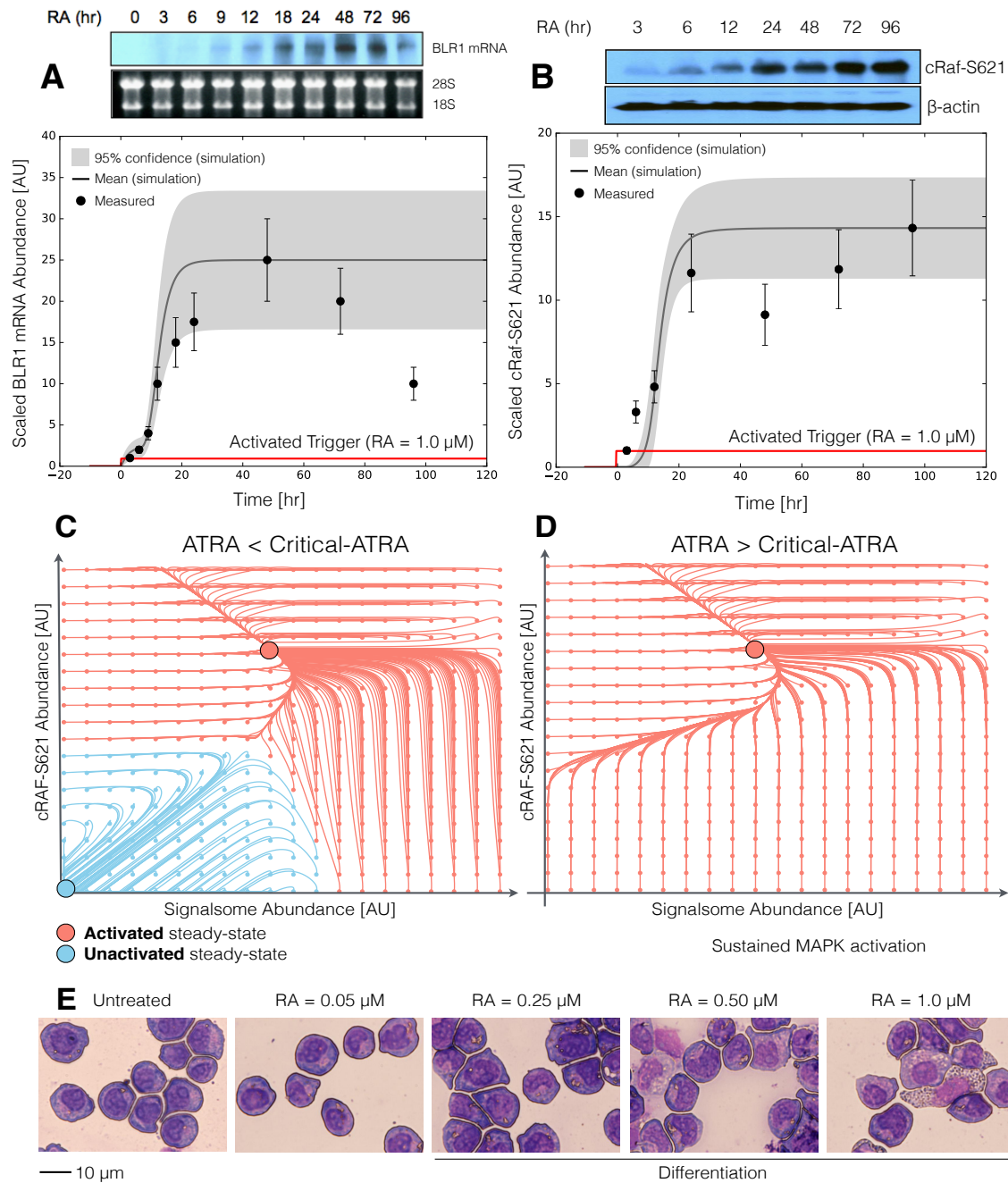


Fig. 2: Model analysis for ATRA-induced HL-60 differentiation. A: BLR1 mRNA versus time following exposure to $1\mu\text{M}$ ATRA at $t = 0$ hr. B: cRaf-pS621 versus time following exposure to $1\mu\text{M}$ ATRA at $t = 0$ hr. Points denote experimental measurements, solid lines denote the mean model performance. Shaded regions denote the 99% confidence interval calculated over the parameter ensemble. C: Signalsome and cRaf-pS621 nullclines for ATRA below the critical threshold. The model had two stable steady states and a single unstable state in this regime. D: Signalsome and cRaf-pS621 nullclines for ATRA above the critical threshold. In this regime the model had only a single stable steady state. E: Morphology of HL-60 as a function of ATRA concentration ($t = 72$ hr).

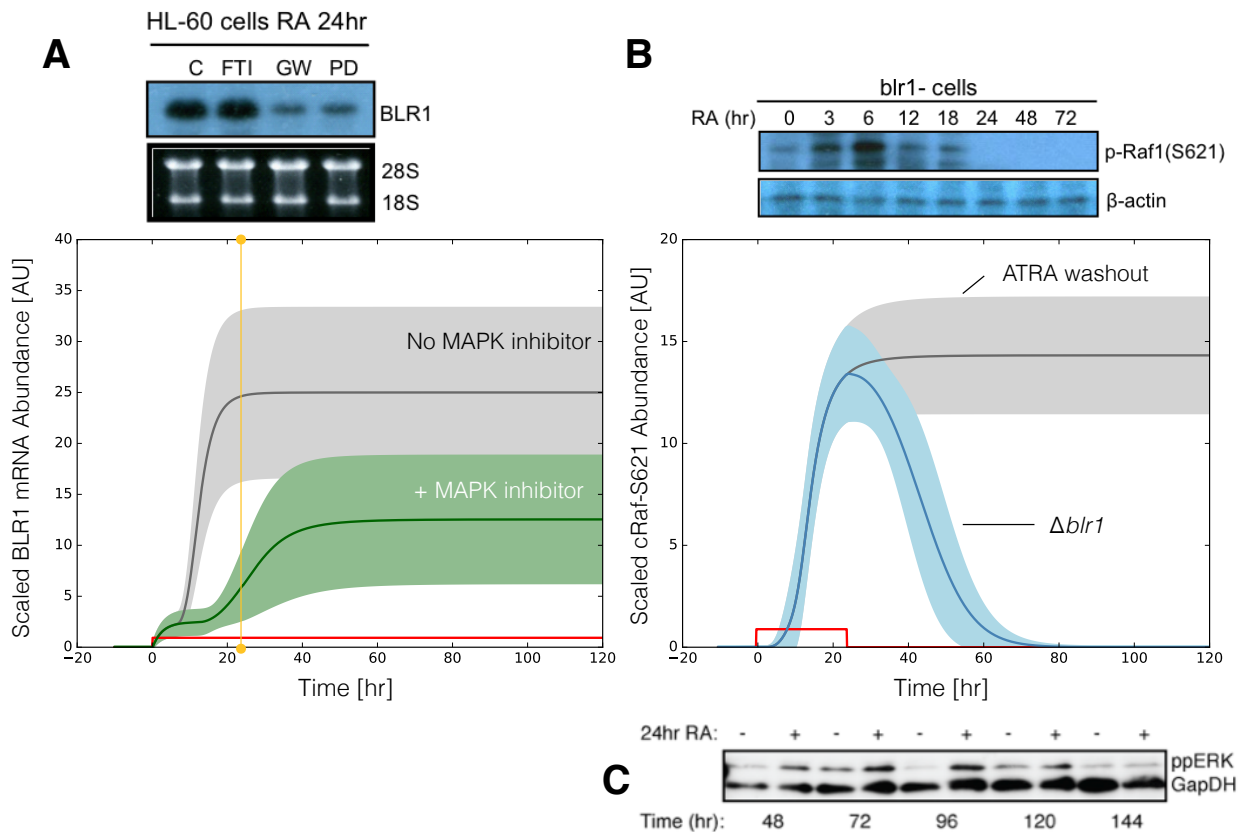


Fig. 3: Model simulation following exposure to $1\mu\text{M}$ ATRA. A: BLR1 mRNA versus time with and without MAPK inhibitor. B: cRaf-pS621 versus time following pulsed exposure to $1\mu\text{M}$ ATRA with and without BLR1. Solid lines denote the mean model performance, while shaded regions denote the 99% confidence interval calculated over the parameter ensemble. C: Western blot analysis of phosphorylated ERK1/2 in ATRA washout experiments. Experimental data in panels A and B were reproduced from Wang and Yen (20), data in panel C is reported in this study.

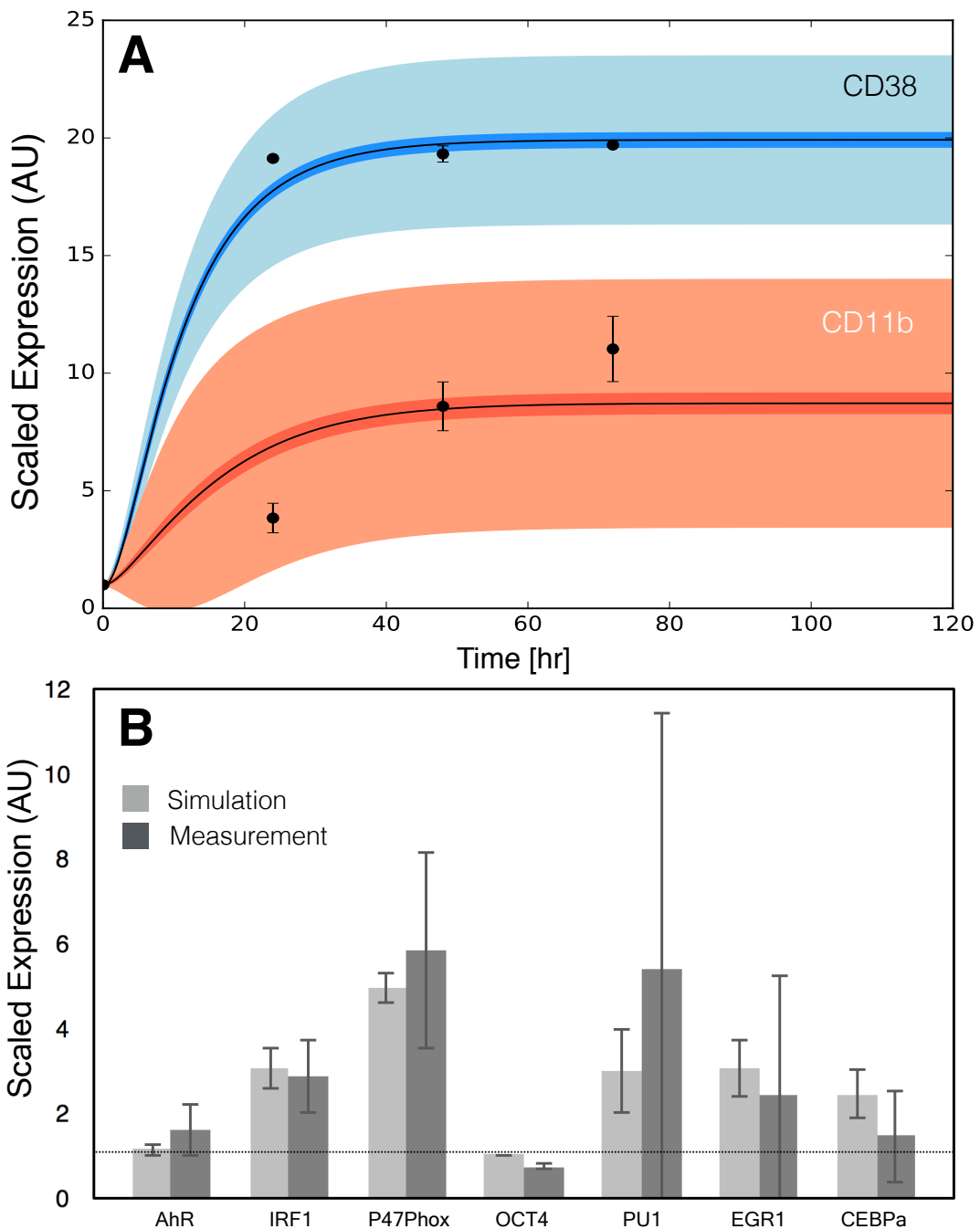


Fig. 4: Model simulation of the HL-60 gene expression program following exposure to $1\mu\text{M}$ ATRA at $t = 0$ hr. A: CD38 and CD11b expression versus time following ATRA exposure at time $t = 0$ hr. B: Gene expression at $t = 48$ hr following ATRA exposure. Experimental data in panels A and B were reproduced from Jensen et al. (48).

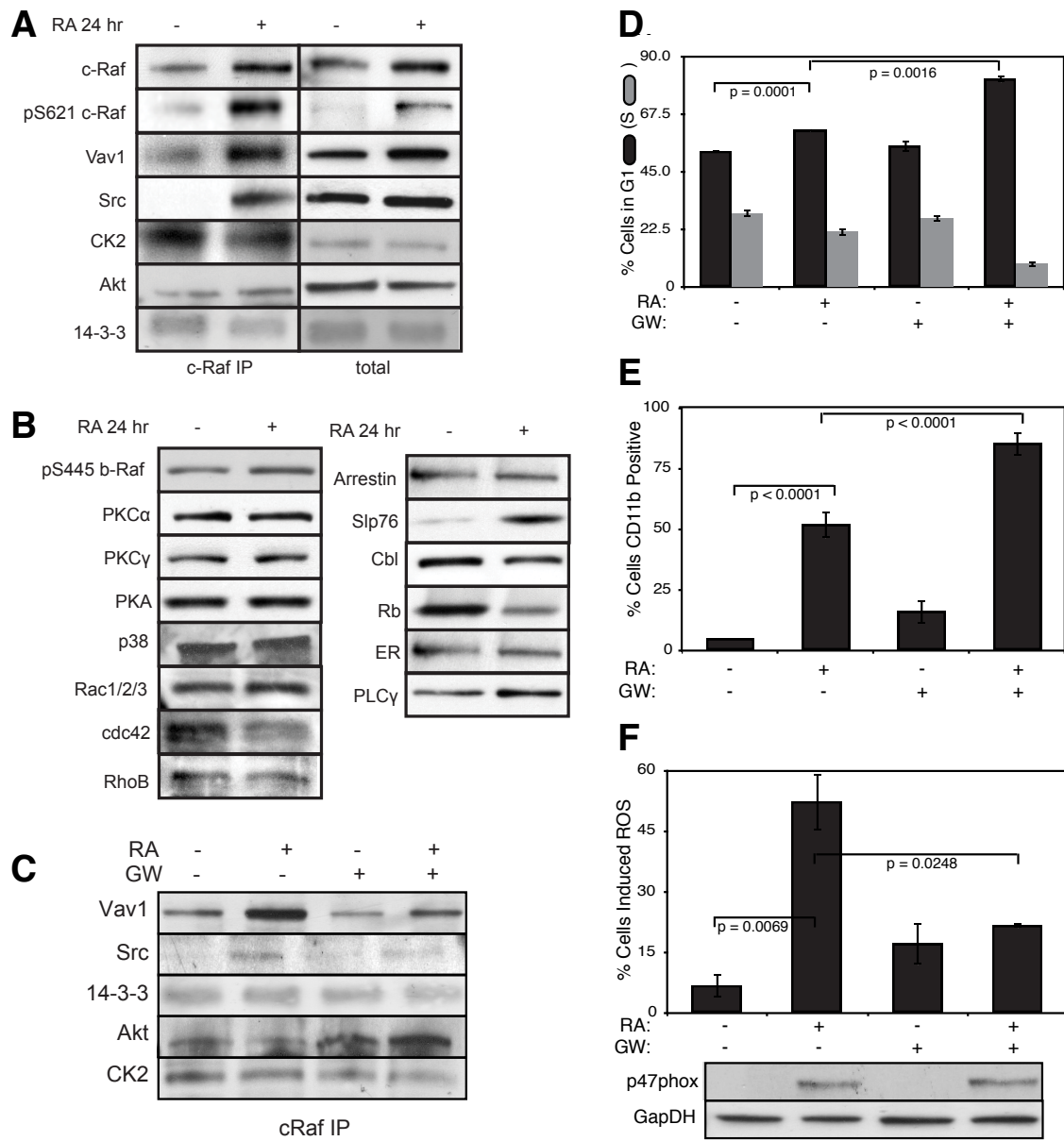


Fig. 5: Investigation of a panel of possible Raf interaction partners in the presence and absence of ATRA. A: Species identified to precipitate out with Raf: first column shows Western blot analysis on total Raf immunoprecipitation with and without 24 hr ATRA treatment and the second on total lysate. B: The expression of species considered that did not precipitate out with Raf at levels detectable by Western blot analysis on total lysate. C: Effect of the Raf inhibitor GW5074 on Raf interactions as determined by Western blot analysis of total Raf immunoprecipitation. The Authors note the signal associated with Src was found to be weak. D: Cell Cycle distribution as determined by flow cytometry indicated arrest induced by ATRA, which was increased by the addition of GW5074. E: Expression of the cell surface marker CD11b as determined by flow cytometry indicated increased expression induced by ATRA, which was enhanced by the addition of GW5074. F: Inducible reactive oxygen species (ROS) as determined by DCF flow cytometry. The functional differentiation response of ATRA treated cells was mitigated by GW5074.